Coupled modeling of well and reservoir for geo-energy applications

Pour, Kiarash Mansour; Voskov, Denis; Bruhn, David

DOI
10.1016/j.geoen.2023.211926

Publication date
2023

Document Version
Final published version

Published in
Geoenergy Science and Engineering

227 (2023) 211926

Contents lists available at ScienceDirect

Geoenergy Science and Engineering

journal homepage: www.sciencedirect.com/journal/geoenergy-science-and-engineering

Coupled modeling of well and reservoir for geo-energy applications

Kiarash Mansour Pour [a], Denis Voskov [a,b,*], David Bruhn [a,c]

[a] Department of Geoscience and Engineering, TU Delft, Delft, Netherlands
[b] Department of Energy Resources Engineering, Stanford University, CA, USA
[c] GFZ German Research Centre for Geosciences, Helmholtz Center Potsdam, Postdam, Germany

ARTICLE INFO

Keywords:
Geothermal simulation
Coupled reservoir and wellbore
Operator-based linearization
Multisegmented well

ABSTRACT

The energy transition is inevitable since approximately two-thirds of the current global GHG emissions are related to energy production. Subsurface can provide a great opportunity for innovative low-carbon energy solutions such as geothermal energy production, hydrogen storage, carbon capture, and sequestration, etc. Well and borehole operations play an important role in all these applications. In order to operate wells intelligently, there must be a robust simulation technology that captures physics and the expected production scenario. In this study, we design a numerical framework for predictive simulation and monitoring of injection and production wells based on the general multi-segment well model. In our simulation model, wells are segmented into connected control volumes similar to the finite-volume discretization of the reservoir. Total velocity serves as an additional nonlinear unknown and it is constrained by the momentum equation. Moreover, transforming nonlinear governing equations for both reservoir and well into linearized equations benefits from operator-based linearization (OBL) techniques and reduce further the computational cost of simulation. This framework was tested for several complex physical kernels including thermal compositional multiphase reactive flow and transport. The proposed model was validated using a comparison with analytic and numerical results.

1. Introduction

Borehole operations are a key component for the management of any energy-related subsurface activities such as energy storage, geothermal energy production, CO_2 sequestration, oil and gas production, wastewater disposal, and thermal recovery processes. Recently, intelligent wells such as long deviated multi-lateral wells with sophisticated inflow control valves have been used to maximize both the economy of the field and the reliability of the operation. Besides, various wellbore designs are used for the efficient production of heat from the subsurface in advanced geothermal approaches. The design, prediction, and optimization of all the processes of interest in energy production require accurate fully-coupled models for thermal multi-phase flow in both the reservoir and the boreholes.

There are multiple challenges with the adequate modeling of such wells. Firstly, capturing accurately the physics (thermal, multiphase flow, multi-component) in the wellbore is complex. Moreover, chemical interactions between the wellbore and flowing fluids cannot be ignored in energy transition applications. The coupling between the wellbore and the reservoir introduces additional complications. The complexity stems from the fact that the flow through the wellbore does not follow Darcy's law. This means that the momentum equation must be solved considering pressure losses due to friction, acceleration, and gravitational forces acting in the fluid. Moreover, the model should be reliable enough to honor more sophisticated intelligent well topology.

Several coupled reservoir and well models were proposed to simulate the complex physics present in the wellbore. The most common approach for modeling a well in reservoir simulation is the standard well model that considers the well as a point source or sink term in the perforated reservoir block (Peaceman, 1990). However, the standard well model is blind to the actual physics of the wellbore. Moreover, it cannot capture the complex well network topology which may include chokes, valves, and various surface facilities. To overcome the above drawback, the multisegmented well (ms-well) model was proposed (Holmes et al., 1998; Schlumberger, 2007; Jiang, 2008). In the ms-well model, the borehole is discretized into several segments with the fluid velocity, node pressure, and other properties simulated along with the wellbore geometry. The benefits of the general ms-well model are its flexible approximation of the actual geometry of each wellbore and its handling of the complex well topology and controls in the pipeline network. Moreover, introducing velocity as an additional degree of freedom allows us to account for various pressure losses by solving the momentum equation.

* Corresponding author at: Department of Geoscience and Engineering, TU Delft, Delft, Netherlands.
E-mail address: D.V.Voskov@tudelft.nl (D. Voskov).

https://doi.org/10.1016/j.geoen.2023.211926
Received 31 March 2023; Received in revised form 9 May 2023; Accepted 13 May 2023
Available online 26 May 2023

Multiple solution strategies for coupled reservoir and well models were proposed in the literature. Livescu et al. (2008) proposed a semianalytical thermal multiphase wellbore-flow model for general-purpose simulation. Pan and Oldenburg (2014) proposed the hybrid implicit (semi-explicit) solution for the transient momentum equation in the geothermal wellbore. In addition, a few fully coupled numerical models with different strategies for thermal wellbore flow have been suggested (Holmes et al., 1998; Jiang, 2008; Livescu et al., 2010). All these models operate at various simplifying assumptions for wellbore physics and wellbore coupling with the reservoir. There are different formulations for geothermal wellbore simulation exist. Multiple solution strategies for stand-alone geothermal wellbore simulation that neglect wellbore coupling have been recommended. Tonkin et al. (2021) makes an in-depth review of the geothermal wellbore simulation. The analytical solution for coaxial wellbore simulation was suggested by Horne (1980). Besides a limitation in the coupling, most existing strategies exclude chemical interactions.

In this study, we are interested in a fully implicit coupling of the complex Thermal–Hydraulic–Chemical flow model in the wellbore and reservoir due to unconditional stability. In the fully implicit approach, we use Newton's method to linearize and solve a set of nonlinear equations. Linearization of discrete mass and energy governing equations of multiphase, multicomponent flow, and transport is a challenging task due to the highly nonlinear coupling and complex thermodynamic phase behavior that needs to resolve multiphase partitioning of different components at each nonlinear iteration to accurately evaluate the fluid/rock properties (Collins et al., 1992; Voskov and Tchelepi, 2012).

The linearization stage for such problems is always a demanding task due to the complexity of Jacobian assembly in the presence of fully coupled physical–chemical interactions. A new approach for the linearization of governing equations called operator-based linearization (OBL), was proposed by Voskov (2017) following ideas from tie-simplex parametrization (Iranshahr et al., 2013a,b). In this approach, the exact physics kernels of the governing partial differential equations were approximated using abstract algebraic operators. Later this technique was extended and implemented in the open-source Delft Advanced Research Terra Simulator (DARTS, 2023). DARTS is a scalable parallel modeling framework that aims to accelerate the simulation performance while capturing multi-physics geo-application processes such as hydrocarbon production (Lyu et al., 2021c,a), geothermal energy extraction (Khait and Voskov, 2018; Wang et al., 2020) and CO_2 sequestration (Kala and Voskov, 2020; Lyu et al., 2021b; Pour et al., 2023).

In this work, we develop a new computational framework in DARTS applying the general decoupled velocity formulation and extend OBL to couple well and reservoir model. Well and reservoir are both discretized similarly into nodes and connections following the general unstructured grid framework (connection list approach, e.g., Lim, 1995) using the finite volume method. Total velocity serves as an additional nonlinear unknown written at each interface (connection) on the total computational domain and bounded by a suitable momentum equation. Similar to the staggered gridding method, this framework adopts a simultaneous approach by coupling the mass and energy balance equations at the center of each cell with the momentum balance equations at the cell interfaces. Moreover, transforming both reservoir and well nonlinear governing equations into an operator form benefits from OBL techniques and reduce further the computational cost related to linearization.

The paper is organized as follows. First, the governing equations describing thermal, multiphase multi-component flow in the wellbore and the reservoir are presented in detail. Next, we present our decoupled velocity design and OBL solution strategies for solving coupled wellbore and reservoir equations. We first test the accuracy and consistency of the method through a set of benchmark tests. Next, more complex numerical experiments are conducted to take into account a more realistic wellbore coupled with a field model.

2. Governing equations

For the investigated domain with volume Ω, bounded by surface Γ, the mass and energy conservation can be expressed in a uniformly integral way along with the proper momentum equation as shown in the Table 1.

Here, we introduce all terms in the equations as functions of spatial coordinate ξ and physical state $\boldsymbol{\omega}$:

- $\phi(\xi,\boldsymbol{\omega})$- porosity,
- $x_{cj}(\boldsymbol{\omega})$ - mole fraction of component c in phase j,
- $s_j(\boldsymbol{\omega})$ - phase saturations,
- $\rho_j(\boldsymbol{\omega})$- phase molar density,
- $\mathbf{v}_j(\xi,\boldsymbol{\omega})$- phase velocity,
- $U_j(\boldsymbol{\omega})$ - phase internal energy,
- $U_r(\boldsymbol{\omega})$ - rock internal energy,
- $h_j(\boldsymbol{\omega})$ - phase enthalpy,
- κ - thermal conduction.

Next, we formulate a one-dimensional momentum balance equation for the entire fluid in the wellbore. Assuming the coordinate z points along the well, this equation is given by Hibiki and Ishii (2003) and Issa and Kempf (2003).

$$\frac{\partial p^w}{\partial z} = -\rho_m g - \frac{\partial p^w}{\partial t}(\rho_m V_m) - \frac{\partial(\rho_m V_m^2)}{\partial z} - \frac{f_{tp}\rho_m V_m^2}{2d_{in}} - R_m \tag{1}$$

We focus on well momentum equation in Table 1, where $\rho_m(\boldsymbol{\omega})$ is the total mixture density, g is the gravitational acceleration in the z direction, d_{in} is the internal diameter of the well, where f_{tp} is the friction factor, which is a function of the dimensionless Reynolds number Re (ratio of inertial forces to viscous forces), d is the diameter of the segment, and V_m is the velocity of the fluid mixture in the segment.

$$f_{tp} = \begin{cases} 16/Re, & Re \le 2000 \text{ (laminar flow)} \\ 1/\left(-3.6\log\left(\frac{6.9}{Re} + (\frac{\epsilon}{3.7d})^{\frac{10}{9}}\right)\right)^2, & Re \ge 4000 \text{ (Torbulent flow)} \\ 16/2000 + k_f(R_e - 2000), & 2000 < Re < 4000 \end{cases} \tag{2}$$

The general momentum equation (1) can be simplified to the steady state momentum equation as follows

$$\frac{\partial p^w}{\partial z} = (\frac{\partial p}{\partial z})_h + (\frac{\partial p}{\partial z})_f + (\frac{\partial p}{\partial z})_a. \tag{3}$$

The equation above simply states the total pressure loss over any control volume (segment) of the well as the sum of three components' forces (acceleration, friction, and hydrostatic).

The momentum equation for the reservoir part is simplified to Darcy's law, and phase velocity is computed as:

$$v_j = -\frac{\mathbf{K}k_{rj}}{\mu_j}(\nabla p_j - \rho_j g \nabla d). \tag{4}$$

where

- $\mathbf{K}(\xi)$ – permeability tensor,
- $k_{rj}(\boldsymbol{\omega})$ – relative permeability,
- $\mu_j(\boldsymbol{\omega})$ – phase viscosity,
- $\boldsymbol{p}_j(\boldsymbol{\omega})$ – vector of pressures in phase j,
- $\rho_j(\boldsymbol{\omega})$ – phase density,
- $d(\xi)$ – vector of depths (positive downwards).

3. OBL solution strategy with decoupled velocity formulation

Unlike the conventional DARTS formulation, in which the problem's primary unknowns were written on the cell centers and velocity was not

Table 1
Mass, energy and momentum balance equations.

Description	Equation
Conservation of mass and energy	$\frac{\partial}{\partial t}\int_{\Omega} M^k d\Omega + \int_{\Gamma} F^k.nd\Gamma = \int_{\Omega} q^k$
Mass accumulation	$M^k(\omega, v_m) = \phi \sum_{j=1}^{n_p} x_{cj}\rho_j s_j$
Energy accumulation	$M^{ke}(\omega, v_m) = \phi \sum_{j=1}^{n_p} x_{cj}\rho_j s_j U_j - (1-\phi)U_r$
Mass flux	$F^k(\xi, \omega, v_m) = \sum_{j=1}^{n_p} x_{cj}\rho_j v_j$
Energy flux	$F^{ke}(\xi, \omega, v_m) = \sum_{j=1}^{n_p} x_{cj}\rho_j v_j h_j + \kappa\nabla T$
Reservoir momentum equation	$v_j = -\frac{\mathbf{K}k_{rj}}{\mu_j}(\nabla p_p - \rho_j g\nabla D)$
Well momentum equation	$\frac{\partial p^w}{\partial z} = -\rho_m g - \frac{\partial p^w}{\partial t}(\rho_m V_m) - \frac{\partial(\rho_m V_m^2)}{\partial z} - \frac{f_{tp}\rho_m V_m^2}{2d_{in}} - R_m$

one of them, the decoupled velocity formulation considers velocity as an additional nonlinear unknown (state) of the problem written at each interface between two nodes. On each node, the following independent variables are defined:

- $\omega = [\ p_i, h_i, \mathbf{z}_i\ ]$ which corresponds to pressure, enthalpy, and the vector of overall molar fractions respectively.

Note that the above variables are all defined at the center of the node. On each connection, we define total velocity:

- v_m, Total velocity

3.1. Governing equations for fully coupled approach

After discretizing governing Table 1, using the finite volume scheme and backward Euler approximation in time, we transform the mass and energy residuals into an operator form as follows:

$$R_{nm}(\omega, v) = V_n\phi\Big(\alpha_c(\omega) - \alpha_c(\omega^n)\Big) + \Delta t\sum_l \beta_c^l(\omega)v_m^l(\xi, \omega) = 0. \tag{5}$$

In Eq. (5), operators read as:

$$\beta_c(\omega) = \sum_j x_{cj}f_j\rho_j, \tag{6}$$

$$\alpha_c(\omega) = \big(1 + c_r(p - p_{ref})\big)\sum_j x_{cj}\rho_j s_j, \tag{7}$$

The discretized energy conservation equation in operator form can be written as:

$$\begin{aligned} R_{ne}(\boldsymbol{\omega}, v) &= V_n\phi\Big(\alpha_f(\boldsymbol{\omega}) - \alpha_f(\boldsymbol{\omega}^n)\Big) + (1-\phi)V_nU_r\Big(\alpha_{er}(\boldsymbol{\omega}) - \alpha_{er}(\boldsymbol{\omega}^n)\Big) \\ &+ \Delta t\sum_l \beta_e^l(\boldsymbol{\omega})v_m^l(\xi, \boldsymbol{\omega}) \\ &+ \Delta t\sum_l \Gamma^l(T_i - T_j)\Big(\phi_0\gamma_{ef}(\boldsymbol{\omega}) + (1-\phi_0)k_r\alpha_{er}(\omega)\Big) = 0. \end{aligned} \tag{8}$$

$$\beta_e(\boldsymbol{\omega}) = \sum_j x_{cj}f_j\rho_j h_j, \tag{9}$$

$$\alpha_f(\boldsymbol{\omega}) = \Big(1 + c_r(p - p_{ref})\Big)\sum_j x_{cj}\rho_j s_j U_p, \tag{10}$$

$$\alpha_{er}(\boldsymbol{\omega}) = \frac{1}{1 + c_r(p - p_{ref})}, \tag{11}$$

$$\gamma_{ef} = \Big(1 + c_r(p - p_{ref})\Big)\sum_j s_j k_j, \tag{12}$$

The momentum equations are defined at the interface (connections of two nodes). For each connection between node block i and j, we write a discrete momentum equation in residual form as follows depending on the connection whether it is between wells or reservoir blocks.

$$\mathbf{R}_c = \begin{cases} v_{mix} + T_c\lambda(\omega)(P_i - P_j), & \text{reservoir connection,} \\ P_i - P_j - (\Delta P_h + \Delta P_f + \Delta P_h), & \text{well connection.} \end{cases} \tag{13}$$

In the Darcy velocity equation (13), T_c is the transmissibility and $\lambda(\boldsymbol{\omega})$ is the total mobility operator of the upwind grid block. For the momentum equation in a wellbore, ΔP^w is the pressure drop between two nodes, and ΔP_h^w, ΔP_f^w and ΔP_a^w are the hydrostatic, frictional and acceleration components of the pressure drop, respectively. For simplicity, we only take into account the friction losses. The frictional pressure difference between two nodes is defined as

$$\Delta P_f^w = \Big(\frac{2f_{tp}\rho^{seg}V_m^2}{d}\Big)\Delta x_i, \tag{14}$$

where f_{tp} is the friction factor which is a function of the dimensionless Reynolds number Re (ratio of inertial forces to viscous forces) explained previously, d is the diameter of the segment, and V_m is the velocity of the fluid mixture in the segment connection.

The hydrostatic pressure difference between two nodes is:

$$\Delta P_h^w = \rho_t g\Delta H, \tag{15}$$

Acceleration pressure losses are given by the following formula:

$$\Delta P_a^w = \frac{2m_{in}V_m}{A}, \tag{16}$$

where $m_{in} = \sum_p \rho_p(\omega)Q_p$ is the mass flow rate of the mixture entering the segment defined as

$$m_{in} = \sum_i^{Nperf}\Big(WI(p_u^w - p_{perf})\lambda(\omega)\rho_{tot}(\omega)\Big)_i, \tag{17}$$

where ΔH is the height difference between two nodes and ρ_t is the total mass density. p_u^w is the pressure of the upwind node for connection c between two well segments and P_{Perf} is the pressure in the perforated reservoir block.

3.2. Solution of equations

The fully coupled method is a commonly used method to solve coupled problems implicitly. In this method, equations for all the subproblems are solved simultaneously. We assemble our global Jacobian matrix based on the variables defined on each node and connection

$$\begin{cases} R_N(\omega^{n+1}, \boldsymbol{v}_t^{n+1}) = 0, & \text{Node equations;} \\ R_C(\omega^{n+1}, \boldsymbol{v}_t^{n+1}) = 0, & \text{Connection equations.} \end{cases} \tag{18}$$

Newton's method is applied to the entire system and the Newton update can be obtained by solving a single linear system:

$$\begin{bmatrix} J_{NN} & J_{NC} \\ J_{CN} & J_{CC} \end{bmatrix}\begin{bmatrix} \delta\omega \\ \delta\boldsymbol{v}_t \end{bmatrix} = -\begin{bmatrix} R_N \\ R_C \end{bmatrix}, \tag{19}$$

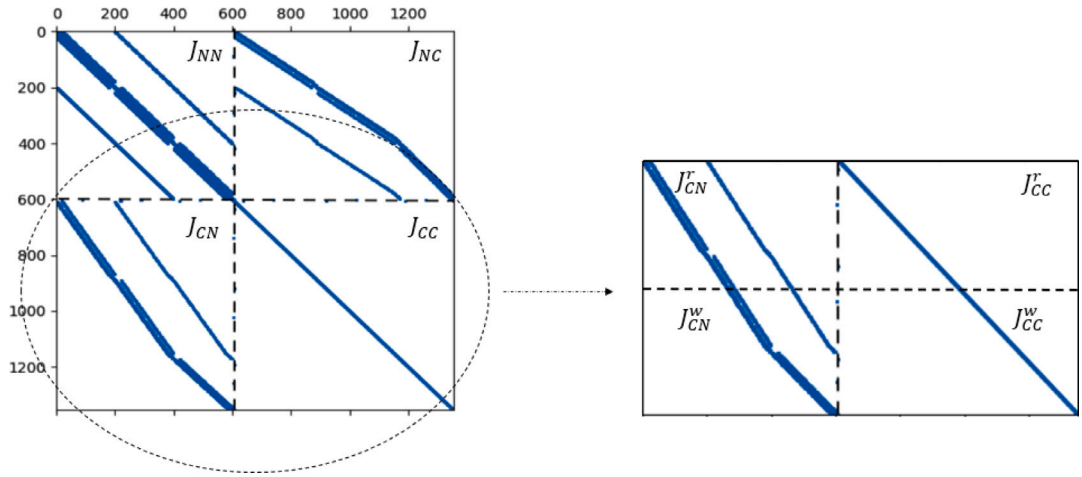

Fig. 1. Decoupled velocity Jacobian matrix for 3-D reservoir, zooming into momentum equation part.

where matrices J_{NN}, J_{CN} corresponds to derivatives with respect to node unknowns ω^{n+1} and J_{NC}, J_{NN} correspond to derivatives with respect to v_t^{n+1} respectively.

The coupled system will be solved until reaching the global convergence criteria:

$$\begin{cases} \|R_N(\omega^{n+1}, \boldsymbol{u}_t^{n+1})\| < \epsilon_n, & \text{Node equations;} \\ \|R_C(\omega^{n+1}, \boldsymbol{u}_t^{n+1})\| < \epsilon_c, & \text{Connection equations.} \end{cases} \tag{20}$$

We subdivide the node equations and connection equations of the reservoir into the node or well parts and define the specific tolerance for each subdomain as follows

$$\begin{cases} \|R_{NR}(\omega^{n+1}, \boldsymbol{u}_t^{n+1})\| < \epsilon_{nr}, & \text{Node equations for reservoir blocks} \\ \|R_{NW}(\omega^{n+1}, \boldsymbol{u}_t^{n+1})\| < \epsilon_{nw}, & \text{Node equations for well blocks} \\ \|R_{CR}(\omega^{n+1}, \boldsymbol{u}_t^{n+1})\| < \epsilon_{cr}, & \text{Connection equations for reservoir interfaces} \\ \|R_{CW}(\omega^{n+1}, \boldsymbol{u}_t^{n+1})\| < \epsilon_{cw}, & \text{Connection equations for well interfaces} \end{cases} \tag{21}$$

The global Jacobian matrix for a decoupled velocity engine is shown in Fig. 1. The global Jacobian matrix has a multilevel matrix structure. It can be divided into two parts at the first level. The upper row is related to the derivatives of the node variables, while the lower row is related to the derivatives of the connection variables. Each part in the second level can be further subdivided into the reservoir part and the well parts. Fig. 1 shows how the matrix can be further subdivided into connection equations with respect to the reservoir and well parts by zooming in on the momentum parts.

While treating velocity as an additional degree of freedom can be computationally expensive, it is necessary to accurately model regions that deviate from Darcy velocity, such as the wellbore. Using decoupled velocity in both reservoir and wellbore allows us consistently translate the pressure gradient in a fully implicit manner. Decoupled velocity formulation allows for an application of different momentum equations, like Darcy–Forchheimer or Darcy–Brinkman, in the near-well reservoir region.

3.3. General well pipeline modeling

Ms-well is discretized into nodes and connections in a similar fashion to a reservoir using a finite-volume scheme. Any well segment can be connected with an arbitrary number of reservoir control volumes, representing well perforations. We write the control equation either as a pressure control also known as BHP control for the ghost cell (Fig. 2) or we write it as rate control and solve it for the first connection as follows:

$$\begin{cases} R_1^{seg} = \omega_1^{seg} - \omega_{target}, & \text{BHP control} \\ R_1^{conn} = \frac{v_j^{s,j}}{\rho_j^{sc}} \cdot (\sum_c \sum_p \rho_p Q_p x_{x,p}) - Q_j^{target}, & \text{Rate control} \end{cases} \tag{22}$$

As shown in Fig. 2, each well segment can have zero, one, or multiple perforations. Each segment of the ms-well wellbore is a separate object that can have different geometrical properties from other segments. Currently, in DARTS, two types of tube and annulus segments are available as shown in Fig. 3.

4. Numerical results

We test the proposed implementation by comparing it with analytical solutions or numerical results using conventional simulation techniques.

4.1. Verification of heat loss model

In this test, we validate our numerical model with the analytical heat loss model in which the overall resistance of the well is calculated with an analogy to the resistance circuits as follows (Fontanilla, 1980).

$$R_{total} = \frac{1}{2\pi L}\left(\frac{1}{h_f r_i} + \frac{1}{\lambda_p} ln(\frac{r_o}{r_i}) + \frac{1}{h_p r_o} + \frac{1}{\lambda_{ins}} ln(\frac{r_{ins}}{r_o}) + \frac{1}{h_{rc} r_{ins}}\right), \tag{23}$$

$$q = \frac{(\Delta T)_{total}}{R_{total}}, \tag{24}$$

Here h_f is the heat transfer coefficient of heat transfer between the fluid inside the pipe and the wall, h_{pi} is the coefficient of heat transfer across any deposits of scale and dirt at the inside wall of the pipe and insulation, r_i is the inner radius of the pipe, r_0 is the outer radius of the pipe and essentially the inner radius of the insulation, r_{ins} is the external radius of the insulation, and λ_p and λ_{ins} are the thermal conductivities of the pipe and insulation, q is the overall heat loss.

In figure. 4. We mimic the well–bore connection to the reservoir with different resistance materials. In Fig. 4.b we compare the numerical solution vs analytical solution of the temperature profile due to the heat losses. It can be seen that both solutions match quite close.

4.2. Simple 3D reservoir with ms-well

In this test case, the reservoir dimension is 3 × 10 × 10 (taking from SPE1 benchmark, see Odeh, 1981) with lateral permeabilities of K_{xy} = 100, and 500 mD, while the vertical permeability was set as $Kz = K_{xy}/100$. We inject water in pressure 405 bar and produce oil.

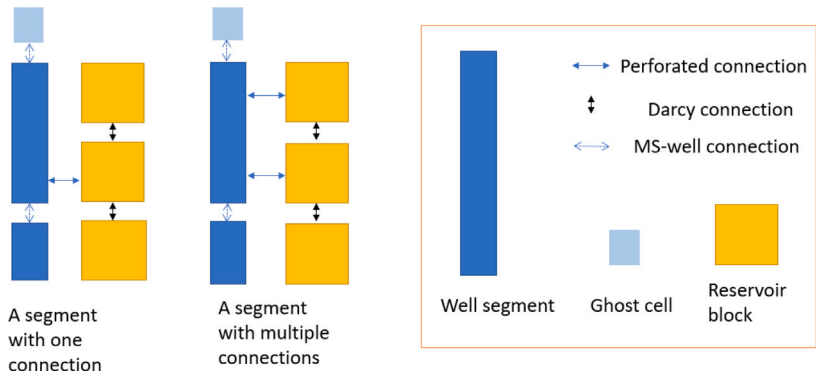

Fig. 2. Ms-well–reservoir network schematic.

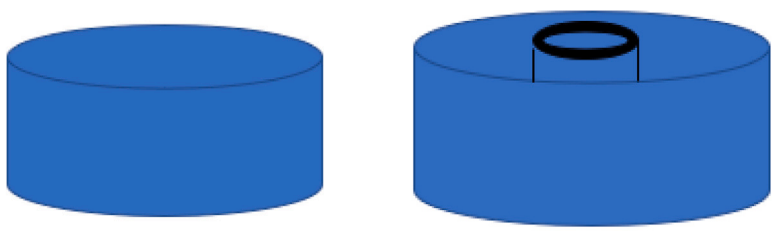

(a) Tube pipe (b) Annulus pipe

Fig. 3. Well segment type.

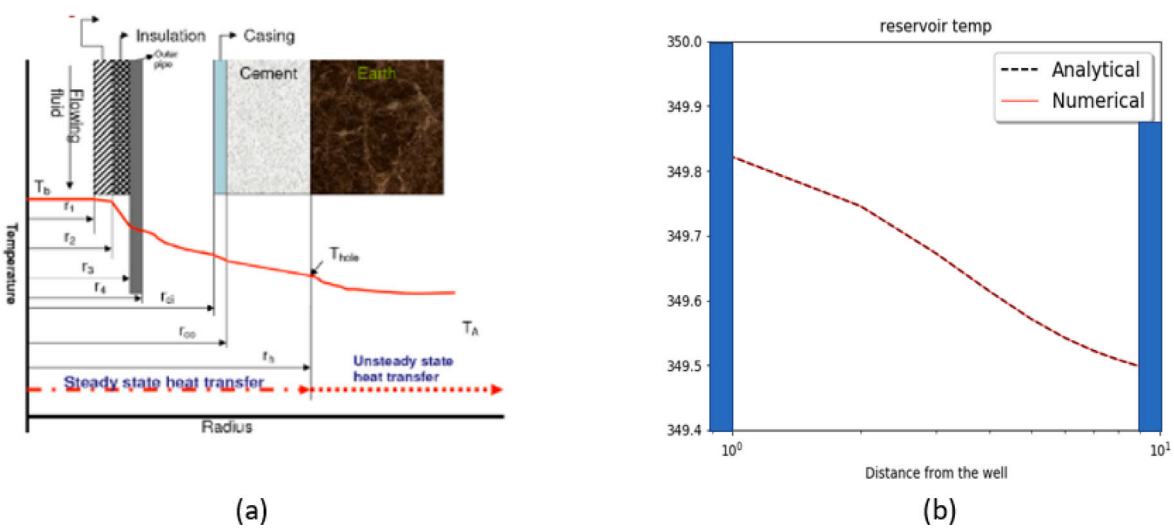

Fig. 4. (a) wellbore–reservoir heat losses schematic and (b) comparison of analytical model (Prats, 1986) vs numerical solutions.

the reservoir is initially in 400 pressure bar and we produce at 395 bar for the producing well. Two vertical multi-segmented wells with three segments each are placed at the opposite corners of the model. Each segment is connected to the corresponding layer with different well indices 10, 20, and 30 (see Fig. 5).

Initially, the reservoir is saturated with oil at 400 bar. We inject water in the injection ms-well at 405 pressure and produce at 395 bar at the production ms-well. We run the simulation for 4000 days. The comparison between DARTS and AD-GPRS with the ms-well model is shown in Figs. 6. From this graph, we can observe that there is a perfect match between both DARTS and ADGPRS for this model. You can see that the breakthrough happens quite quickly in the model following the most permeable layer and gradually increasing while oil production is following a backward trend. Due to the changing mobility, the injection rate is growing non-monotonically. Notice that the production rate is shown in negative volume when the injection rate is shown in positive. Fig. 7 compares the snapshot of the water overall molar fraction profile at time 80 days in the production well segments. Here again, we compare solutions produced by ADGPRS and DARTS. Except for a small difference in segment 2, all results are matching quite close. Finally, in Fig. 8 we compare the performance of DARTS vs ADGPRS. In both simulators, a nonlinear tolerance of 10^{-3} is set for mass and momentum conservation. For this test case, the nonlinear solver using Newton's method and the local chop of overall fractions with a maximum allowable update of 0.1 is selected for both ADGPRS and DARTS. In DARTS, the direct SUPERLU solver is used to obtain the

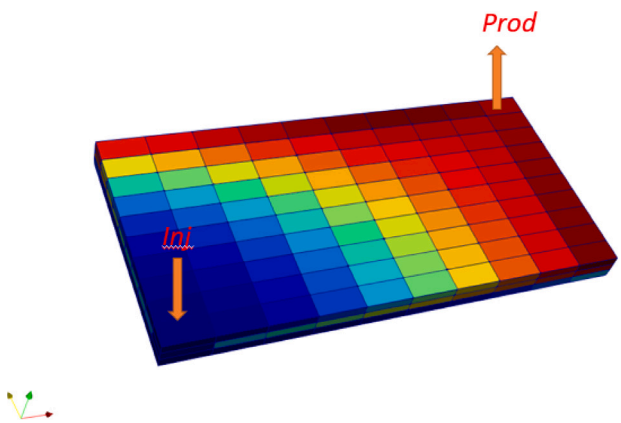

Fig. 5. Coupled Reservoir-ms-well model.

Table 2
Comparison between decoupled velocity and conventional well formulation in DARTS with pseudo porous media assumptions.

DARTS formulation	Nonlinear iteration	CPU time[sec]
Pseudo-porous medium	73	8.44
Decoupled velocity	160	21.4

Table 3
Simulation parameters for reactive transport test case.

Parameter	Value
Initial porosity ϕ_0 [-]	0.26
Initial pressure, p_0 [bar]	95
Initial overall fraction $[H_2O, Ca^{2+} + CO_3^{-2}, CaCO_3]$	[0.09, 0.01, 0.8901]
Injection overall fraction $[H_2O, Ca^{2+} + CO_3^{-2}, CaCO_3]$	[0.8, 0.01, 0.18]
Solubility constant, K_{sp}[-]	55
Simulation time, t [days]	1.8e5
Injection pressure, BHP_{inj} [bar]	135
Production pressure, BHP_{prod} [bar]	65

linear solution for decoupled velocity formulations. In order to make a fair comparison, a similar setting was employed in ADGPRS.

We can see that the number of Newton iterations and CPU time are lower in DARTS which can be explained by the utilization of molar nonlinear formulation and the OBL approach.

4.3. Heterogeneous low-enthalpy geothermal model

In this test case, we show the capabilities of the decoupled velocity engine for the simulation of a geothermal reservoir with heterogeneous properties. A single-layer model extracted from a synthetic geological setting of the West Netherlands Basin Wang et al. (2020) is chosen here. The model has dimensions of 60 × 40 × 1 and a grid size of 30 m × 30 m × 1 m. Two horizontal multi-segmented wells with 10 segments each are placed at the left and right center of the model. Fig. 9 illustrates the permeability and porosity distribution as well as locations of the model. The initial pressure of the reservoir is 200 bar, with a temperature of 348 K. We inject water at 308 K with a constant pressure of 250 bars and produce with BHP control at 125 bars.

Fig. 10(a) shows the pressure and enthalpy distribution after 3650 days and compares it with the conventional DARTS engine without considering velocity as an additional nonlinear unknown following approach suggested in Moridis et al. (2022). In this approach, the wellbore is discretized and modeled using Darcy's law. As we can see, a good match is obtained using this approach conventional DARTS engine with an error of less than 0.05%. Fig. 10(b) compares the well temperature profile along the wellbore comparing the solution using ms-well with the solution using a simplified well model. It is clear that for conventional (near steady-state) geothermal simulation, the pseudo-porous medium approach is accurate enough and can be used instead of the more expensive ms-well approach with a decoupled momentum equation.

In Table 2, we compare the performance of decoupled velocity formulation with ms-well vs conventional DARTS formulation using a pseudo-porous medium approach. We can see that the number of nonlinear iterations and CPU time are lower in the case of the conventional approach. The primary reason for this is that the decoupled velocity approach involves an additional degree of freedom with respect to velocity, increasing each iteration's computational cost. Furthermore, the conventional approach typically requires fewer nonlinear iterations because of the simplified momentum equation.

4.4. Reactive transport test case

One of the major impacts in geothermal systems is related to reactive transport. Precipitation inside the geothermal well can influence heavily the production results. Moreover, dissolution in the near-wellbore area due to acidification can, on the contrary, increase productivity. All these processes involve the chemical alternation of fluid and solid components near or inside the wellbore. Currently, the implemented ms-well technology is only tested with the dissolution model in DARTS and in this test, we demonstrate the capability of the DARTS framework.

Here we use the decoupled velocity with an unstructured mesh and demonstrate how it can capture the near-wellbore dissolution of carbonates. For this test case, we analyze the dissolution of calcite which can be written as a simple kinetic equation:

$$CaCO_3 \leftrightarrow Ca^{2+} + CO_3^{2-}, \tag{25}$$

We treat this reaction as an equilibrium one. The equilibrium relations are defined by the law of mass action and are given as

$$Q - K_q = \prod_{c=1}^{C} \alpha_c^{c_{eq}} - K_q = 0 \tag{26}$$

Here, α_c is the activity of component c, Q_q is the reaction quotient and K_q is the equilibrium reaction quotient or equilibrium solubility limit in the case of dissolution/precipitation of minerals. The rigorous description of reactive transport modeling in DARTS is described in Kala and Voskov (2020). The injection well is perforating the left boundary and the production well is located on the right boundary of the reservoir.

The model has a dimension of 100 by 100 m. A constant permeability of 1mD is used with random noise of 5%. Fig. 11(a) shows both the permeability of the reservoir and the locations of the wells and Fig. 11(b) shows the unstructured grid domain of the model. The proposed model aims to simulate the phenomenon of unstable wormhole formation that occurs due to minor permeability perturbations near the injector wellbore. The reservoir features an injector well on one side that is perforated across its entire thickness, and a producer well on the other side, spanning the entire thickness of the reservoir. This example model has dimensions of 100 meters by 100 m. Table 3 specifies the simulation parameter for this test case. Fig. 12 illustrates the solution of solid overall molar fraction $CaCO_3$ at 3 three different times: 0.13 t_d, 0.25 t_d, and at t_d where t_d is the dimensionless time.

It is clear that chemical interactions can be incorporated into the developed ms-well extension of the DARTS framework. In future work, we are going to implement precipitation of minerals in the wellbore and near-well reservoir to accurately capture injectivity decline in the geothermal wells.

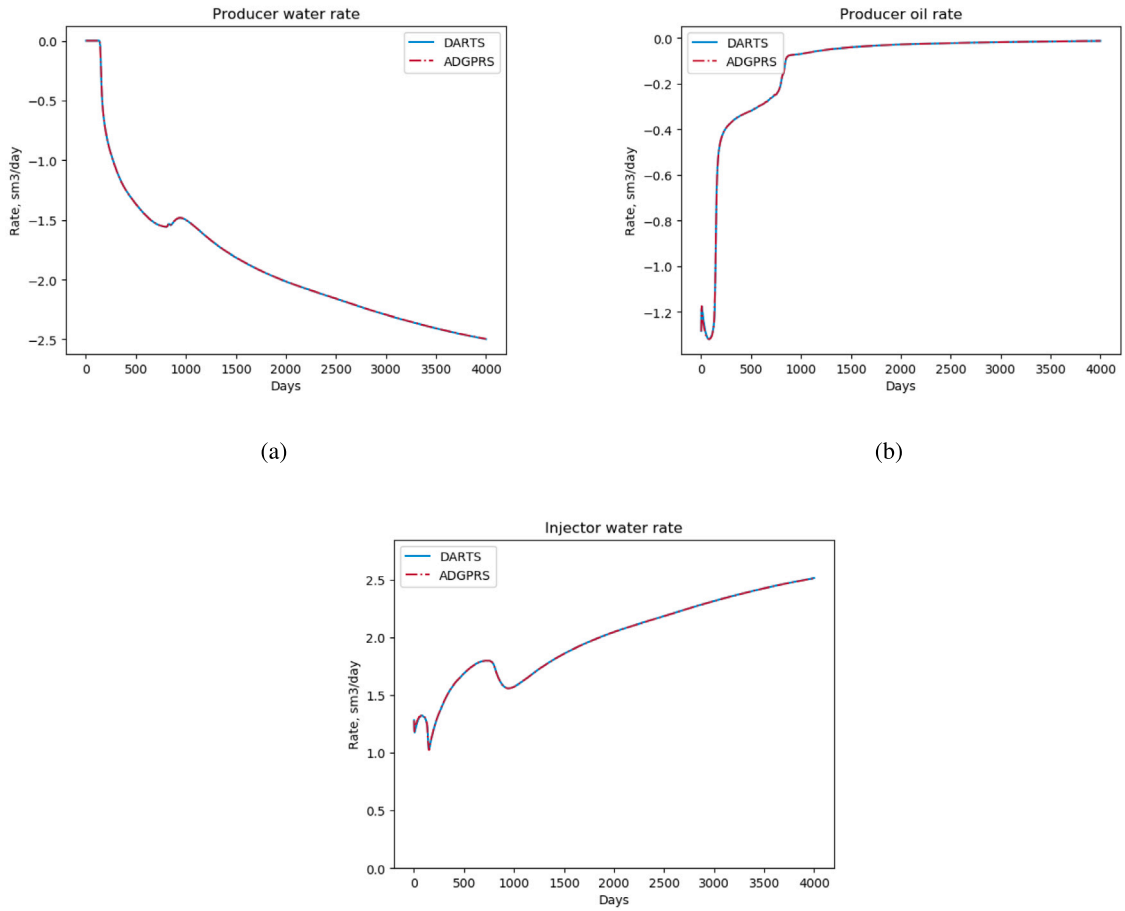

Fig. 6. Benchmark testcase with ADGPRS for SPE1 reservoir.

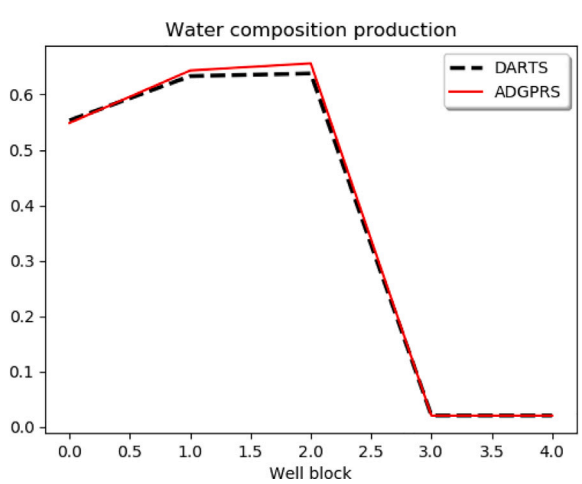

Fig. 7. Water overall molar fraction inside the wellbore after 80 days.

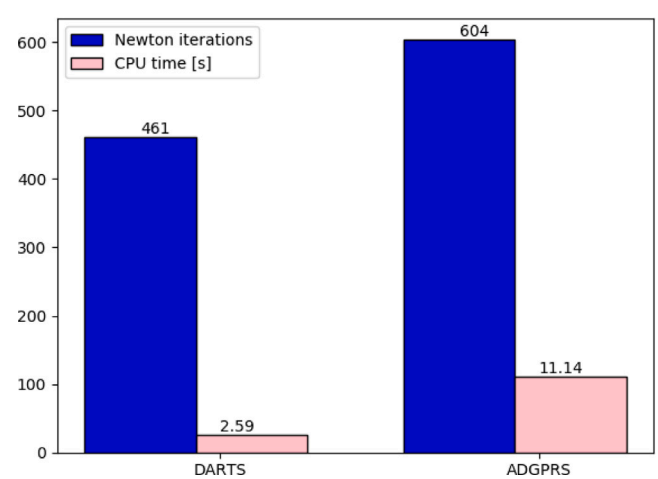

Fig. 8. Performance comparison between DARTS and AGPRS.

4.5. Closed-loop wellbore model

In this example, we will test the developed framework for modeling advanced geothermal setups. Fig. 13 schematically illustrates a single closed-loop also known as coaxial wellbore setup. In order to, model such wells, the wellbore is discretized into nodes and connected to the reservoir using a finite-volume scheme. Any well segment can be connected with an arbitrary number of reservoir control volumes, representing conductive heat flux. There are currently two types of tube and annulus segments available in DARTS that allow us to model

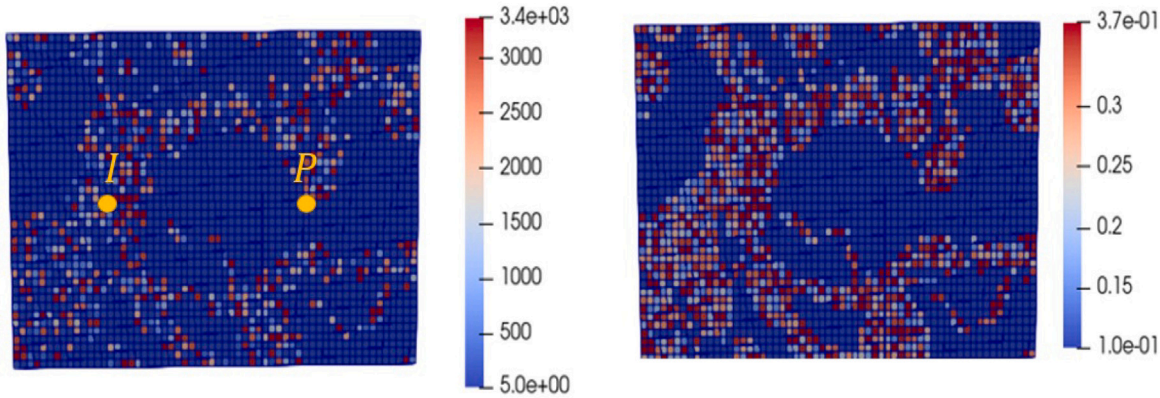

Fig. 9. Permeability (right figure) and porosity distribution with well locations (left figure).

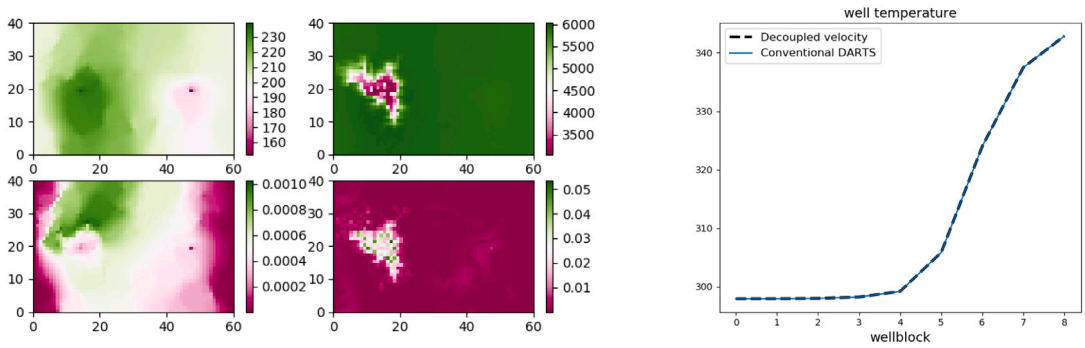

(a) (b)

Fig. 10. (a) Comparison 2-D heterogeneous pressure and low enthalpy solution obtained with the decoupled velocity and the pseudo-porous medium approach (b) Temperature profile along the wellbore for both approaches.

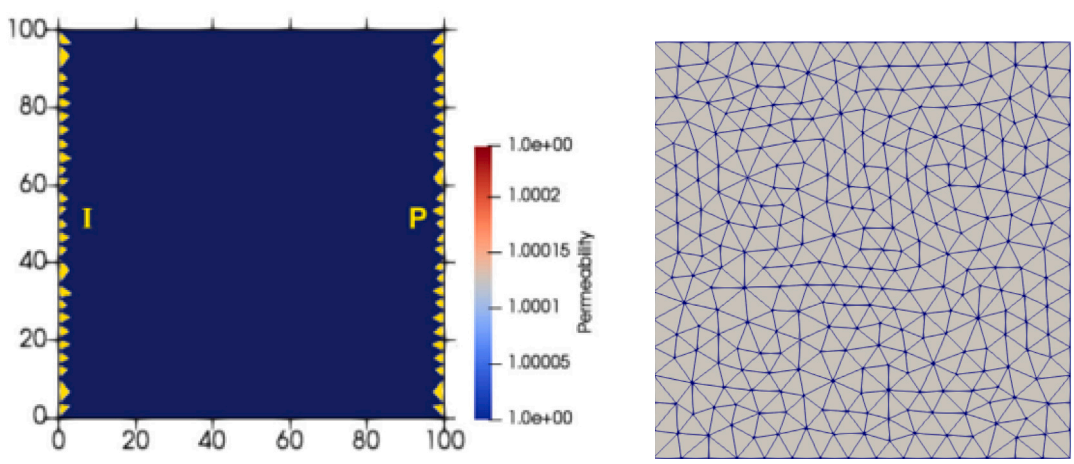

(a) (b)

Fig. 11. (a) Reservoir permeability map with specified well locations and (b) discretization mesh.

coaxial wellbores. In order to model such well, we need to create a special connection list. Fig. 14 schematically illustrates the discretized wellbore and corresponding connection list for such wells.

We made two different scenarios for two different flow directions and investigate the effect of the heat conduction (different resistance) between the annulus and the reservoir part. In this test case, the reservoir dimensions are $1 \times 1 \times 100$ with a grid of size $0.30 \times 30 \times 6.96$ m with impermeable layers. The ms-well with 100 segments for annulus and the inner tube is fully (conductively) connected to the 100 reservoir blocks. We ran the test case for 2.4 h while taking into account various conductive heat transfer coefficients, t_d between the annulus and the

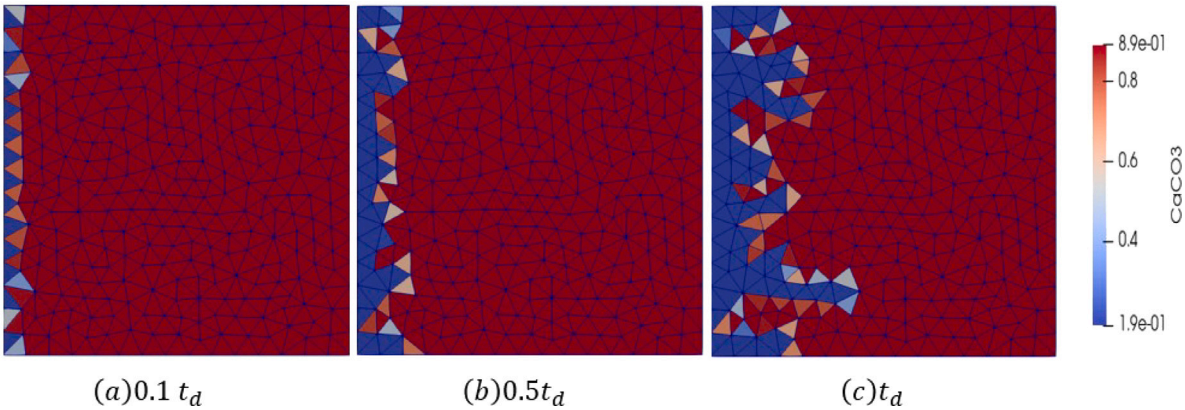

Fig. 12. Calcium Carbonate dissolution of the wormhole model at three different time snapshots.

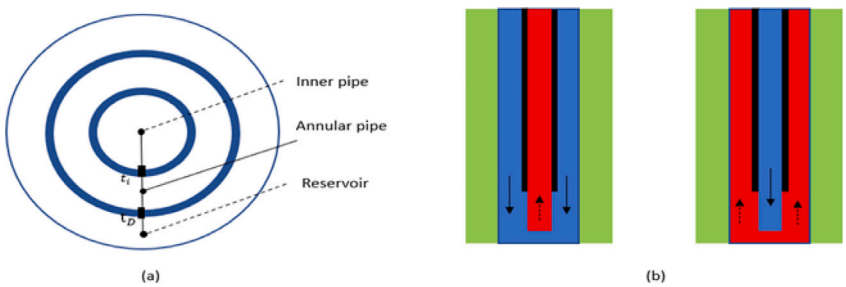

Fig. 13. (a) Cross section of a pipe-in-pipe single closed-loop wellbore (b) schematic diagram of a single-well closed loop for different flow direction.

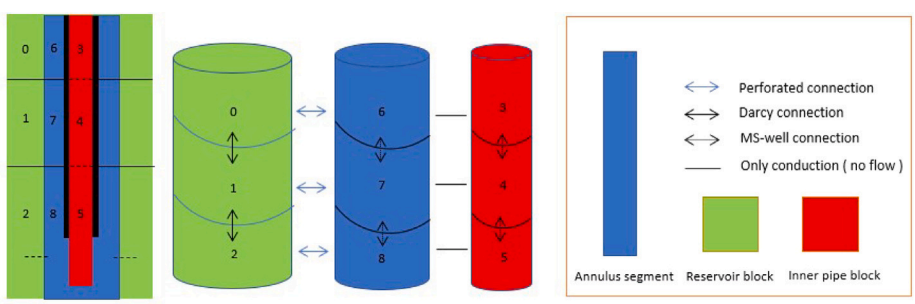

Fig. 14. Connection list of the coaxial wellbore network.

reservoir. In this test case, we also assume a perfect insulation between the annulus and the inner tube ($t_i = 0$).

In Fig. 15 we can see the temperature profile along the annulus and the inner tube while we inject from the annulus and produce from the inner tube. We can see that by increasing the t_d the temperature profile goes slightly upward, meaning lower resistance between the annulus and the reservoir and thus more heat conduction. Fig. 16 corresponds to the reverse flow direction in which we inject from the inner tube and produce from the annulus. As we can see there is no effect of the t_d on the injection well as there is no contact between the inner tube and the reservoir. On the other hand, the temperature profile along the annulus is nonlinear and temperature increases by increasing the conductivity between the annulus and the reservoir. The obtained solution qualitatively follows the results reported in Chen et al. (2019) for a similar coaxial setup.

5. Conclusion

We have developed a new computational framework that can simulate Thermal–Hydraulic–Chemical (THC) multiphase multi-component fully-coupled flow in the wellbore and the reservoir. The implementation is based on an operator-based linearization (OBL) method used in Delft Advanced Research Terra Simulator (DARTS). In the OBL approach, the governing equations are represented in operator form which significantly simplifies the solution of highly nonlinear governing equations with complex physics. In the proposed framework, the OBL technique is extended to both the governing equations of the reservoir and the wellbore. During the simulation, multilinear interpolation is used to interpolate the corresponding values and derivatives of operators, which reduces the computational cost related to linearization. Our simulation model is built on a general unstructured grid framework, in which the wellbore is divided into segments that follow a similar scheme as the finite-volume discretization used for the reservoir. The total velocity serves as an additional nonlinear unknown that is constrained by the momentum equation, allowing for writing a suitable momentum equation for a wellbore.

First, we verify the accuracy of the ms-well model by comparing a solution for thermal, two-phase immiscible physics with Automatic Differentiation General Purpose Research Simulator (ADGPRS). Our test produces comparable results to an accurate ms-well model in both simulation frameworks. The performance comparison of DARTS

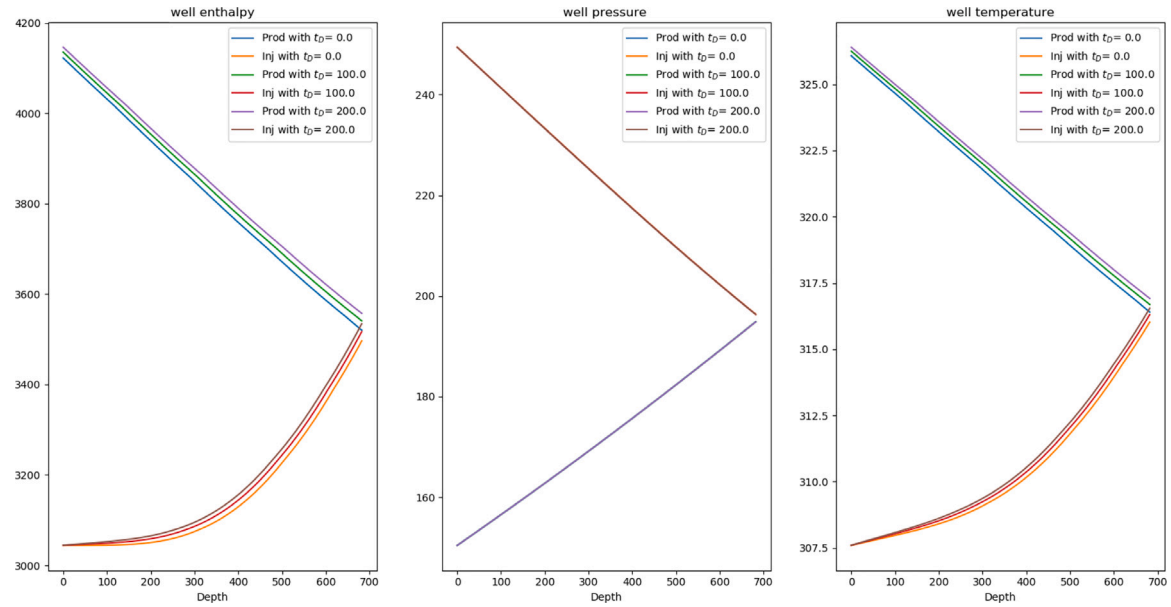

Fig. 15. Comparison of water temperature profile under different thermal conductivity between annulus and reservoir while injecting from annulus pipe.

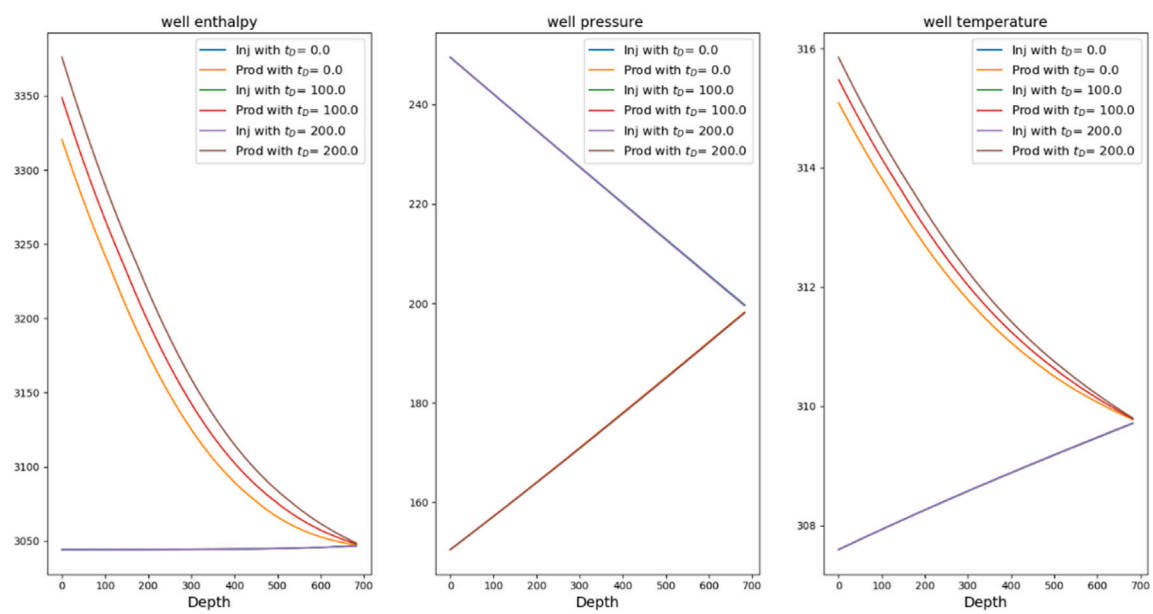

Fig. 16. Comparison of water temperature profile under different thermal conductivity between annulus and reservoir while injecting from inner pipe.

and ADGPRS simulation shows that DARTS allows for less CPU time and nonlinear iterations due to the different nonlinear formulation and OBL approach. We further test the framework for more complex physics considering thermal effects. We assess the engine's performance for geothermal physics using a heterogeneous reservoir and compare the results to the conventional method with a pseudo-porous medium approach. For cases when transient effects can be ignored, a pseudo-porous medium approach produces a solution comparable to the accurate well model with a lower computational cost. Besides, we test the developed framework in modeling the calcite dissolution in the near-well region on unstructured mesh and the results show that the framework could capture the dissolution effect near the wellbore. Accurate discretization of the wellbore allows us to model sophisticated well technologies such as co-axial wellbores. We made a test case for a single closed loop wellbore and ran multiple numerical experiments and sensitivity analyses on various factors that affect heat extraction from the co-axial wellbore.

Our study has identified several promising areas for future research. One potential direction is to extend the drift-flux model for multiphase flow in the wellbore into an operator form and integrate more complex chemical interactions in both the wellbore and reservoir. Another promising area is to investigate the development of an iterative linear solver for a decoupled velocity engine on both CPU and GPU platforms. The nonlinear nature of coupled wellbore and reservoir simulations with complex physical models can cause the nonlinear solver to struggle and slow down the convergence process. Therefore, developing a nonlinear solver for this framework is an important future direction of our research. Extending the Trust-region method, which is integrated into the operator-based linearization framework, to include both the

coupled wellbore and reservoir simulations would be a promising direction to pursue. Furthermore, decoupled velocity formulation separates the momentum equation from mass and energy, as well as the well and reservoir regions, providing a promising solution for developing a local nonlinear solver that can identify areas with convergence issues and resolve them. Additionally, we aim to extend the model to include more advanced well-network topologies, taking into account surface capabilities, chokes, and valves.

Declaration of competing interest

The authors declare that they have no known competing financial interests or personal relationships that could have appeared to influence the work reported in this paper.

Data availability

Data will be made available on request.

Acknowledgments

We would like to acknowledge the entire DARTS team for their constructive suggestions.

References

Chen, C., Shao, H., Naumov, D., Kong, Y., Tu, K., Kolditz, O., 2019. Numerical investigation on the performance, sustainability, and efficiency of the deep borehole heat exchanger system for building heating. Geotherm. Energy 7 (1), http://dx.doi.org/10.1186/s40517-019-0133-8.

Collins, D., Nghiem, L., Li, Y.-K., Grabonstotter, J., 1992. An efficient approach to adaptive- implicit compositional simulation with an equation of state. SPE Reserv. Eng. 7 (02), 259–264. http://dx.doi.org/10.2118/15133-PA.

DARTS, 2023. Open Delft Advanced Research Terra Simulator. GitLab, GitLab Repository.

Fontanilla, J.P., 1980. A Mathematical Model for the Prediction of Wellbore Heat Loss and Pressure Drop in Steam Injection Wells. PRISM, http://dx.doi.org/10.11575/PRISM/10182.

Hibiki, T., Ishii, M., 2003. One-dimensional drift–flux model for two-phase flow in a large diameter pipe. Int. J. Heat Mass Transfer 46 (10), 1773–1790. http://dx.doi.org/10.1016/S0017-9310(02)00473-8.

Holmes, J., Barkve, T., Lund, O., 1998. Application of a multisegment well model to simulate flow in advanced wells. In: Proceedings of the European Petroleum Conference, Vol. 2. pp. 171–181. http://dx.doi.org/10.2118/50646-ms.

Horne, R.N., 1980. Design considerations of a down-hole coaxial geothermal heat exchanger. In: Transactions - Geothermal Resources Council, Vol. 4.

Iranshahr, A., Voskov, D.V., Tchelepi, H.A., 2013a. A negative-flash tie-simplex approach for multiphase reservoir simulation. SPE J. 18 (6), 1140–1149. http://dx.doi.org/10.2118/141896-PA.

Iranshahr, A., Voskov, D.V., Tchelepi, H.A., 2013b. Tie-simplex based compositional space parameterization: Continuity and generalization to multiphase systems. AIChE J. 59 (5), 1684–1701. http://dx.doi.org/10.1002/aic.13919.

Issa, R., Kempf, M., 2003. Simulation of slug flow in horizontal and nearly horizontal pipes with the two-fluid model. Int. J. Multiph. Flow. 29 (1), 69–95. http://dx.doi.org/10.1016/S0301-9322(02)00127-1.

Jiang, Y., 2008. Techniques for modeling complex reservoirs and advanced wells (Ph.D. thesis). Stanford University.

Kala, K., Voskov, D., 2020. Element balance formulation in reactive compositional flow and transport with parameterization technique. Comput. Geosci. 24 (2), 609–624.

Khait, M., Voskov, D., 2018. Operator-based linearization for efficient modeling of geothermal processes. Geothermics (ISSN: 0375-6505) 74, 7–18. http://dx.doi.org/10.1016/j.geothermics.2018.01.012.

Lim, K.-T., 1995. A new approach for residual and Jacobian arrays construction in reservoir simulators. http://dx.doi.org/10.2118/16976-PA.

Livescu, S., Durlofsky, L., Aziz, K., 2008. A semianalytical thermal multiphase wellbore flow model for use in reservoir simulation. In: Proceedings - SPE Annual Technical Conference and Exhibition, Vol. 4. pp. 2345–2360. http://dx.doi.org/10.2118/115796-ms.

Livescu, S., Durlofsky, L., Aziz, K., Ginestra, J., 2010. A fully-coupled thermal multiphase wellbore flow model for use in reservoir simulation. J. Pet. Sci. Eng. 71 (3–4), 138–146. http://dx.doi.org/10.1016/j.petrol.2009.11.022.

Lyu, X., Khait, M., Voskov, D., 2021a. Operator-based linearization approach for modeling of multiphase flow with buoyancy and capillarity. SPE J. 26 (4), 1858–1878. http://dx.doi.org/10.2118/205378-PA.

Lyu, X., Voskov, D., Rossen, W.R., 2021b. Numerical investigations of foam-assisted CO2 storage in saline aquifers. Int. J. Greenhouse Gas Control 108, 103314. http://dx.doi.org/10.1016/j.ijggc.2021.103314.

Lyu, X., Voskov, D., Tang, J., Rossen, W.R., 2021c. Simulation of foam enhanced-oil-recovery processes using operator-based linearization approach. SPE J. 26 (4), 2287–2304. http://dx.doi.org/10.2118/205399-PA.

Moridis, G.J., Reagan, M.T., Liu, Y., 2022. Numerical simulations in support of a long-term test of gas production from hydrate accumulations on the Alaska North slope: Reservoir response to interruptions of production (Shut-Ins). Energy Fuels 36 (7), 3496–3525. http://dx.doi.org/10.1021/acs.energyfuels.1c04274.

Odeh, A.S., 1981. Comparison of solutions to a three-dimensional black-oil reservoir simulation problem. J. Pet. Technol. 33 (01), 13–25. http://dx.doi.org/10.2118/9723-PA.

Pan, L., Oldenburg, C.M., 2014. T2Well—An integrated wellbore–reservoir simulator. Comput. Geosci. 65, 46–55. http://dx.doi.org/10.1016/j.cageo.2013.06.005, TOUGH Symposium 2012.

Peaceman, D.W., 1990. Interpretation of wellblock pressures in numerical reservoir simulation. Part 3. Off-center and multiple wells within a wellblock. SPE Reserv. Eng. 5 (2), 6p 16976. http://dx.doi.org/10.2118/16976-pa, Society of Petroleum Engineers.

Pour, K.M., Voskov, D., Bruhn, D., 2023. Nonlinear solver based on trust region approximation for CO2 utilization and storage in subsurface reservoir. Geoenergy Sci. Eng. 211698. http://dx.doi.org/10.1016/j.geoen.2023.211698.

Prats, M., 1986. Thermal Recovery. In: Society of Petroleum Engineers of AIME.

Schlumberger, 2007. Eclipse Technical Description. Geoquest.

Tonkin, R., O'Sullivan, M., O'Sullivan, J., 2021. A review of mathematical models for geothermal wellbore simulation. Geothermics 97, http://dx.doi.org/10.1016/j.geothermics.2021.102255.

Voskov, D.V., 2017. Operator-based linearization approach for modeling of multiphase multi-component flow in porous media. J. Comput. Phys. 337, 275–288.

Voskov, D.V., Tchelepi, H.A., 2012. Comparison of nonlinear formulations for two-phase multi-component EoS based simulation. J. Pet. Sci. Eng. (ISSN: 0920-4105) 82–83, 101–111. http://dx.doi.org/10.1016/j.petrol.2011.10.012.

Wang, Y., Voskov, D., Khait, M., Bruhn, D., 2020. An efficient numerical simulator for geothermal simulation: A benchmark study. Appl. Energy (ISSN: 0306-2619) 264, 114693. http://dx.doi.org/10.1016/j.apenergy.2020.114693.